PROCEEDINGS OF SCIENCE

The NNLO counterterm contributions to $\mathscr{B}(\bar{B} \to X_s\gamma)$ for an arbitrary charm quark mass

M. Misiak
Institute of Theoretical Physics, Faculty of Physics, University of Warsaw,
02-093 Warsaw, Poland.
E-mail: mikolaj.misiak@fuw.edu.pl

A. Rehman[*]
Institute of Theoretical Physics, Faculty of Physics, University of Warsaw,
02-093 Warsaw, Poland
and
National Centre for Physics, Quaid-i-Azam University Campus, Islamabad 45320, Pakistan.
E-mail: abdur.rehman@fuw.edu.pl, abdur.rehman@ncp.edu.pk

M. Steinhauser[†]
Institut für Theoretische Teilchenphysik, Karlsruhe Institute of Technology (KIT),
76128 Karlsruhe, Germany.
E-mail: matthias.steinhauser@kit.edu

The branching ratio $\mathscr{B}(\bar{B} \to X_s\gamma)$ is known to provide stringent constraints on beyond-SM physics. To match the current experimental accuracy, theoretical predictions must include the $\mathscr{O}(\alpha_s^2)$ QCD corrections. One of such corrections has been calculated so far only in two limiting cases for the charm quark mass: $m_c = 0$ and $m_c \gg m_b/2$. An interpolation between these two limits is used to estimate its size, which significantly contributes to the SM prediction uncertainty. An evaluation of this correction for the physical value of m_c is necessary. Here, we present results for all the necessary ultraviolet counterterm contributions that are relevant for this purpose. Their determination requires calculating two-scale three-loop propagator integrals with unitarity cuts.

12th International Symposium on Radiative Corrections (Radcor 2015)
and LoopFest XIV (Radiative Corrections for the LHC and Future Colliders)
15-19 June, 2015
UCLA Department of Physics and Astronomy Los Angeles, USA

[*]Scheduled speaker who could not arrive due to visa issues.
[†]Actual speaker who presented the scheduled speaker's slides.

PoS(RADCOR2015)049

1. Introduction

Being loop-generated by the quark-level $b \to s\gamma$ flavour-changing neutral current transition in the Standard Model (SM), the inclusive $\bar{B} \to X_s\gamma$ decay is known as a well-established means to constrain parameter spaces of Beyond-SM (BSM) models. Sample Leading Order (LO) diagrams for $b \to s\gamma$ in the SM, multi-Higgs doublet models and the Minimal Supersymmetric Standard Model (MSSM) are shown in Fig. 1. One can see that the SM contribution is of the same perturbative order as the possible BSM ones.

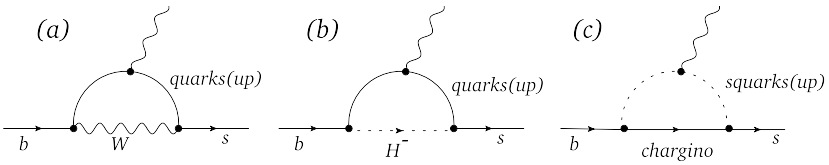

Figure 1: Sample LO diagrams for $b \to s\gamma$ in the SM (a), multi-Higgs doublet models (b), and the MSSM (c).

The present SM prediction for the CP- and isospin-averaged branching ratio of the considered process reads $\mathscr{B}^{\rm SM}_{s\gamma} = (3.36 \pm 0.23) \cdot 10^{-4}$ [1, 2]. It agrees very well with the current experimental world average that, depending on the source, equals to $\mathscr{B}^{\rm exp}_{s\gamma} = (3.43 \pm 0.22) \cdot 10^{-4}$ [3] or $\mathscr{B}^{\rm exp}_{s\gamma} = (3.41 \pm 0.16) \cdot 10^{-4}$ [4]. The resulting 95% C.L. bound on the charged Higgs boson mass in the Two-Higgs-Doublet Model II is in the vicinity of 500 GeV [1, 4].

All the quoted results for the branching ratio correspond to the $E_\gamma > E_0 = 1.6\,\text{GeV}$ cut on the photon energy in the decaying meson rest frame. For larger values of E_0, theoretical calculations would become less precise due to nonperturbative uncertainties that scale with powers of $\Lambda_{\rm QCD}/(m_b - 2E_0)$. On the other hand, the experimental errors grow for smaller E_γ due to subtraction of a larger and more uncertain background. The actual measurements are performed with $E_0 \in [1.7, 2.0]\,\text{GeV}$, and extrapolations in E_0 are performed for evaluation of the world averages. The two above-mentioned averages differ in their approach to the extrapolation.

As far as the SM prediction uncertainty is concerned, it has been obtained by combining in quadrature four types of uncertainties: (i) nonperturbative (5%) [5], (ii) parametric (2%), (iii) higher-order $(\mathscr{O}(\alpha_{\rm s}^3))$ perturbative (3%), and (iv) the one stemming from an interpolation in the charm quark mass that is used to estimate some of the $\mathscr{O}(\alpha_{\rm s}^2)$ corrections (3%) [2].

In the near future, the experimental accuracy is going to improve in a significant manner, after the Belle-II experiment [6] begins collecting data. Consequently, the SM calculations must also be upgraded to match the expected experimental precision.

In the present work, we focus on a calculation that contributes to removing the fourth type of uncertainty, namely the one due to the interpolation in m_c. To define the corrections in question, let us write the perturbative rate of the weak radiative b-quark decay as

$$\Gamma(b \to X_s^{\rm partonic}\gamma) = \frac{G_F^2 m_{b,pole}^5 \alpha_{\rm em}}{32\pi^4} |V_{ts}^* V_{tb}|^2 \sum_{i,j} C_i(\mu_b) C_j(\mu_b) \hat{G}_{ij}, \tag{1.1}$$

where $X_s^{\rm partonic}$ stands for $s, sg, sgg, sq\bar{q}, \ldots$ with $q = u, d, s$. The Wilson coefficients $C_i(\mu_b)$ play the role of coupling constants in the effective Lagrangian $\mathscr{L}_{\rm weak} \sim \sum_i C_i Q_i$ that describes flavour-

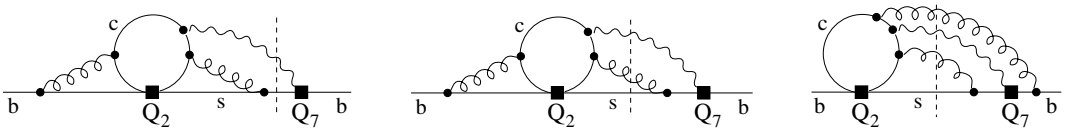

Figure 2: Sample diagrams for $\hat{G}_{27}^{(2)}$ with unitarity cuts indicated by the dashed lines.

changing weak interactions below the W-boson decoupling scale. For our purpose, only three operators Q_i are relevant, namely

$$Q_1 = (\bar{s}_L\gamma_\mu T^a c_L)(\bar{c}_L\gamma^\mu T^a b_L), \qquad Q_2 = (\bar{s}_L\gamma_\mu c_L)(\bar{c}_L\gamma^\mu b_L), \qquad Q_7 = \tfrac{em_b}{16\pi^2}(\bar{s}_L\sigma^{\mu\nu}b_R)F_{\mu\nu}. \quad (1.2)$$

Both α_s and the Wilson coefficients are $\overline{\rm MS}$-renormalized at the low-energy scale $\mu_b \sim m_b/2$ for the decay rate evaluation. The quantities $\hat{G}_{ij}$ in Eq. (1.1) describe interferences of amplitudes generated by the operators Q_i and Q_j. They are perturbatively expanded as follows

$$\hat{G}_{ij} = \hat{G}_{ij}^{(0)} + \widetilde{\alpha}_s\hat{G}_{ij}^{(1)} + \widetilde{\alpha}_s^2\hat{G}_{ij}^{(2)} + \mathscr{O}(\alpha_s^3), \quad (1.3)$$

where $\widetilde{\alpha}_s = \alpha_s(\mu_b)/(4\pi)$. Their global normalization is fixed by the condition $\hat{G}_{77}^{(0)} = e^{\gamma\varepsilon}\Gamma(2-\varepsilon)/\Gamma(2-2\varepsilon)$ in $D = 4-2\varepsilon$ dimensions, with γ denoting the Euler-Mascheroni constant.

Some of the most important Next-to-Next-to-Leading-Order (NNLO) QCD corrections originate from the interference terms $\hat{G}_{17}^{(2)}$ and $\hat{G}_{27}^{(2)}$. These terms depend only on E_0, μ_b and the quark mass ratio $z = m_c^2/m_b^2$, provided the light ($q = u,d,s$) quark masses are neglected. Sample Feynman diagrams contributing to $\hat{G}_{27}^{(2)}$ are shown in Fig. 2. The considered interference is represented there in terms of propagator diagrams with unitarity cuts corresponding to the two-, three- and four-particle final states. Altogether, around 850 of such four-loop diagrams need to be evaluated for generic values of z and E_0, which constitutes an extremely demanding task.

So far, the calculations have been completed only in two limiting cases. In Refs. [7, 8], the quantities $\hat{G}_{17}^{(2)}$ and $\hat{G}_{27}^{(2)}$ were determined for $m_c \gg m_b/2$ and arbitrary E_0. In Ref. [2], the same quantities were evaluated for $m_c = 0$ and $E_0 = 0$. Next, an interpolation between these two limits was performed to arrive at an estimate for the considered correction at the physical value of m_c and with $E_0 = 1.6\,\text{GeV}$. This is illustrated in Fig. 3 where we plot the relative contribution to the branching ratio $\mathscr{B}_{s\gamma}$, namely $U = \left(\Delta\mathscr{B}_{s\gamma}(\sqrt{z},0) - \Delta\mathscr{B}_{s\gamma}(0,0)\right)/\mathscr{B}_{s\gamma}$, with $\Delta\mathscr{B}_{s\gamma}(m_c/m_b,E_0)$ denoting the interpolated part of the NNLO correction to $\mathscr{B}_{s\gamma}$ – see Ref. [2] for more details.

It is evident from Fig. 3 that the interpolated contribution to the branching ratio is sizeable, amounting to around 5% of $\mathscr{B}_{s\gamma}$ at the physical value of m_c/m_b. As already mentioned, the associated uncertainty has been estimated at the $\pm 3\%$ level, which gives a significant contribution to the overall uncertainty of the SM prediction. Thus, efforts to calculate the considered correction for an arbitrary value of m_c should be continued.

2. The z-dependent counterterms for $\hat{G}_{17}^{(2)}$ and $\hat{G}_{27}^{(2)}$

Here, we report on an arbitrary-m_c evaluation of all the necessary ultraviolet-counterterm diagrams that matter for the renormalized $\hat{G}_{i7}^{(2)}$ with $i = 1,2$. Such counterterms need to be added

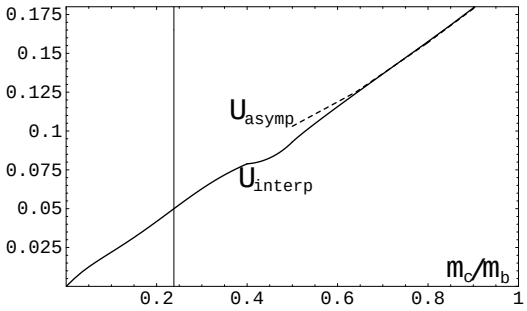

Figure 3: Illustration of the interpolation in m_c (Fig. 4 of Ref. [2]). The solid line describes the interpolated function U (see the text), while the dashed line shows its known asymptotic behaviour for $m_c \gg m_b/2$. The vertical line corresponds to the physical value of m_c/m_b.

to the bare contributions $\hat{G}_{i7}^{(2)\text{bare}}$. A complete renormalization formula for the $z = 0$ case was presented in Section 2.2 of Ref. [2]. Following that approach, we skip charm quark loops on the gluon lines (and the corresponding counterterms), as they are already known from Ref. [9]. Then the renormalization formula for arbitrary z takes the following form:

$$\begin{aligned}
\widetilde{\alpha}_s \hat{G}_{i7}^{(1)} + \widetilde{\alpha}_s^2 \hat{G}_{i7}^{(2)} \;=\; & Z_b^{\text{OS}} Z_m^{\text{OS}} Z_{77} \Big\{ \widetilde{\alpha}_s^2 s^{3\varepsilon} \hat{G}_{i7}^{(2)\text{bare}} + (Z_m^{\text{OS}} - 1) s^{\varepsilon} \Big[Z_{i4} \hat{G}_{47}^{(0)m} + \widetilde{\alpha}_s s^{\varepsilon} \hat{G}_{i7}^{(1)m} \Big] \\
& + \widetilde{\alpha}_s (Z_G^{\text{OS}} - 1) s^{2\varepsilon} \hat{G}_{i7}^{(1)3P} + Z_{i7} Z_m^{\text{OS}} \Big[\hat{G}_{77}^{(0)} + \widetilde{\alpha}_s s^{\varepsilon} \hat{G}_{77}^{(1)\text{bare}} \Big] \\
& + \widetilde{\alpha}_s Z_{i8} s^{\varepsilon} \hat{G}_{78}^{(1)\text{bare}} + \sum_{j=1,\ldots,6,11,12} Z_{ij} s^{\varepsilon} \Big[\hat{G}_{j7}^{(0)} + \widetilde{\alpha}_s s^{\varepsilon} Z_g^2 \hat{G}_{j7}^{(1)\text{bare}} \Big] \\
& + 2\widetilde{\alpha}_s s^{2\varepsilon} (Z_m - 1) z \frac{d}{dz} \hat{G}_{i7}^{(1)\text{bare}} \Big\} + \mathcal{O}(\widetilde{\alpha}_s^3),
\end{aligned} \tag{2.1}$$

It differs from the $z = 0$ case only in the last line where the charm quark mass is renormalized. The l.h.s. of Eq. (2.1) corresponds to $\overline{\text{MS}}$-renormalizing α_s, m_c and the Wilson coefficients at the scale μ_b, while the b-quark mass and the external quark fields are renormalized on-shell. In the on-shell renormalization constants (Eq. (2.8) of Ref. [2]), as well as in Eq. (2.1) here, one should substitute $s = \mu_b^2/m_b^2$. The remaining renormalization constants are the MS-scheme ones (Eq. (2.9) of Ref. [2]), including $Z_m = 1 - 4\widetilde{\alpha}_s/\varepsilon + \mathcal{O}(\widetilde{\alpha}_s^2)$.

The renormalization scale for $\hat{G}_{kl}$ on the r.h.s. of Eq. (2.1) has been set to $\mu^2 = e^{\gamma} m_b^2/(4\pi)$. These quantities involve indices corresponding to the operators listed in Eqs. (1.6) and (2.5) of Ref. [2], in particular to the so-called evanescent ones

$$\begin{aligned}
Q_{11} \;&=\; (\bar{s}_L \gamma_{\mu_1} \gamma_{\mu_2} \gamma_{\mu_3} T^a c_L)(\bar{c}_L \gamma^{\mu_1} \gamma^{\mu_2} \gamma^{\mu_3} T^a b_L) - 16 Q_1, \\
Q_{12} \;&=\; (\bar{s}_L \gamma_{\mu_1} \gamma_{\mu_2} \gamma_{\mu_3} c_L)(\bar{c}_L \gamma^{\mu_1} \gamma^{\mu_2} \gamma^{\mu_3} b_L) - 16 Q_2.
\end{aligned} \tag{2.2}$$

In some of the bare interference terms in Eq. (2.1), the superscript "bare" has been replaced by either "$3P$" or "m", which means that either only the three-particle cuts were included ($3P$), or one of the b-quark propagators was squared (m) for the purpose of the b-quark mass renormalization.

All the necessary bare $\hat{G}_{kl}$ for $z = 0$ can be found in Eqs. (2.3)-(2.7) of Ref. [2]. Only the following ones actually do depend on z: $\hat{G}_{i7}^{(2)\text{bare}}$, $\hat{G}_{i7}^{(1)\text{bare}}$, $\hat{G}_{i7}^{(1)3P}$, $\hat{G}_{i7}^{(1)m}$, for $i = 1, 2$, and

Figure 4: Sample diagrams for $\hat{G}_{27}^{(1)\text{bare}}$ with unitarity cuts indicated by the dashed lines.

$\hat{G}_{7j}^{(1)\text{bare}}$, for $j = 11, 12$. Simple colour-factor considerations imply that $\hat{G}_{17}^{(1)\text{bare}} = -\frac{1}{6}\hat{G}_{27}^{(1)\text{bare}}$, $\hat{G}_{17}^{(1)3P} = -\frac{1}{6}\hat{G}_{27}^{(1)3P}$, $\hat{G}_{17}^{(1)m} = -\frac{1}{6}\hat{G}_{27}^{(1)m}$, and $\hat{G}_{7(11)}^{(1)\text{bare}} = -\frac{1}{6}\hat{G}_{7(12)}^{(1)\text{bare}}$. Moreover, a compact identity relates $\hat{G}_{7(12)}^{(1)\text{bare}}$ to several components of $\hat{G}_{27}^{(1)\text{bare}}$ as follows:

$$\hat{G}_{7(12)}^{(1)\text{bare}} = -4\varepsilon\left\{(1+\varepsilon)\hat{G}_{27}^{(1)2P(d)} + (5+\varepsilon)\left[\hat{G}_{27}^{(1)2P(u)} + \hat{G}_{27}^{(1)3P}\right]\right\}, \tag{2.3}$$

where $\hat{G}_{27}^{(1)2P(d)}$ and $\hat{G}_{27}^{(1)2P(u)}$ denote the two-particle-cut contributions to $\hat{G}_{27}^{(1)\text{bare}}$ that come with the down-type and up-type quark electric charges, respectively.

Thus, what remains to be found for a complete $z \neq 0$ calculation of the counterterm contributions are the six quantities on the r.h.s. of the following two equations:

$$\hat{G}_{27}^{(1)\text{bare}} = \hat{G}_{27}^{(1)2P(d)} + \hat{G}_{27}^{(1)2P(u)} + \hat{G}_{27}^{(1)3P}, \tag{2.4}$$

$$\hat{G}_{27}^{(1)m} = \hat{G}_{27}^{(1)m,2P(d)} + \hat{G}_{27}^{(1)m,2P(u)} + \hat{G}_{27}^{(1)m,3P}. \tag{2.5}$$

They need to be calculated up to $\mathscr{O}(\varepsilon)$. The case of Eq. (2.5) has not been considered so far for arbitrary z. However, Eq. (2.4) is related to Ref. [10] where the NLO calculations of Refs. [11–15] (see Fig. 4) were extended to one more order in ε. In Section 4, we shall compare our results to Ref. [10].

3. Determination and evaluation of the master integrals

To evaluate all the ingredients of Eqs. (2.4) and (2.5), we have reduced the relevant interference terms to Master Integrals (MIs), using the standard Integration-By-Parts (IBP) methods [16–18] implemented in the code `FIRE` [19, 20]. Our MIs are collected in Tab. 1. Dots on the propagators indicate that they are squared. Arrows in I_{16} indicate an irreducible numerator.

After the reduction, each of the considered interference terms becomes a linear combination of the master integrals

$$\begin{aligned}
\hat{G}_{27}^{(1)2P(d)} &= \text{Re}\sum_{k=1}^{8} A_k I_k, & \hat{G}_{27}^{(1)2P(u)} &= \text{Re}\sum_{k=1}^{13} B_k I_k, & \hat{G}_{27}^{(1)3P} &= \text{Re}\sum_{k=14}^{18} C_k I_k, \\
\hat{G}_{27}^{(1)m,2P(d)} &= \text{Re}\sum_{k=1}^{9} D_k I_k, & \hat{G}_{27}^{(1)m,2P(u)} &= \text{Re}\sum_{k=1}^{13} E_k I_k, & \hat{G}_{27}^{(1)m,3P} &= \text{Re}\sum_{k=14}^{18} F_k I_k.
\end{aligned} \tag{3.1}$$

Our explicit expressions for the coefficients $A_k, \ldots F_k$ can be found in Refs. [21, 22].

In our first approach, we numerically evaluate the MIs using the Differential Equation (DE) method [23–25]. The set of MIs in Tab. 1 turns out to be closed under differentiation with respect

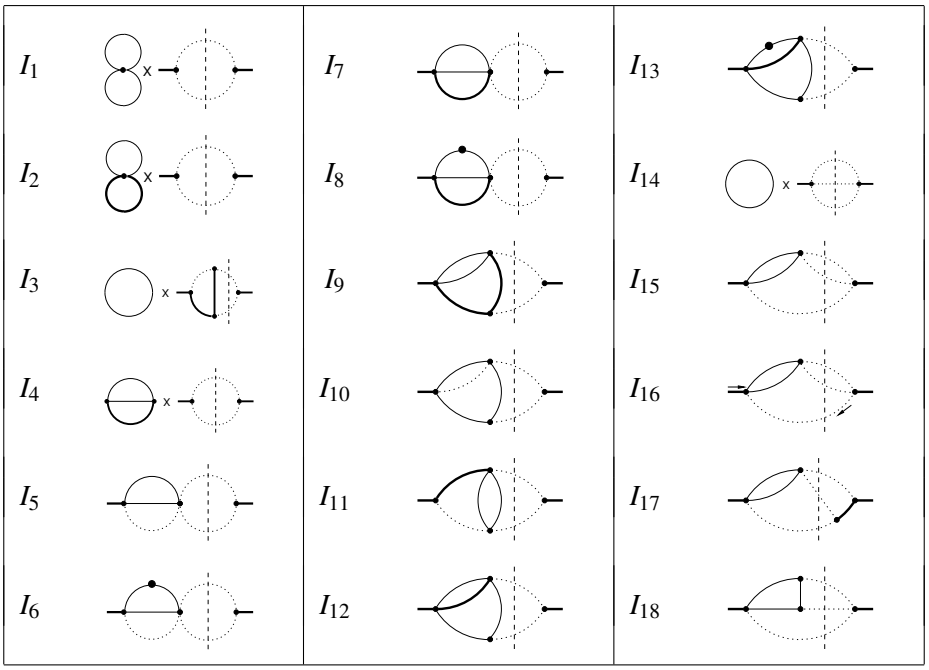

Table 1: Master integrals contributing to the NNLO counterterms with possible two-particle and three-particle cuts indicated by the vertical dashed lines. Thick solid, thin solid and dotted internal lines denote b-quark, c-quark and s-quark propagators, respectively. Thick solid external lines come with the momentum p such that $p^2 = m_b^2$.

to z (if it was not, it could be appropriately extended). In consequence, we obtain a system of differential equations [21, 22] that can be numerically solved starting from initial conditions at large z. It cannot be done along the real axis due to presence of spurious singularities, but rather along ellipses in the complex plane. The initial conditions are found using asymptotic expansions, which effectively reduces our three-loop two-scale problem to a two-loop single-scale one. The asymptotic expansions are evaluated in an automatic manner using the code `exp` [26, 27].

Once the numerical solutions are found, we test them by evaluating the MIs either fully analytically or as expansions in powers of either z or $1/z$. This is achieved with the help of Feynman and Schwinger parameterizations, Mellin-Barnes representations, as well as the DEs themselves for the cases when they can be solved in an analytical manner. The DEs are also used to extend power series in z or $1/z$ to higher orders [21, 22].

4. Results

Our final results are parameterized in terms of eight functions of z as follows

$$\hat{G}_{27}^{(1)2P} \equiv \hat{G}_{27}^{(1)2P(d)} + \hat{G}_{27}^{(1)2P(u)} = -\frac{92}{81\varepsilon} + f_0(z) + \varepsilon f_1(z) + \mathscr{O}(\varepsilon^2), \tag{4.1}$$

$$\hat{G}_{27}^{(1)3P} = g_0(z) + \varepsilon g_1(z) + \mathscr{O}(\varepsilon^2), \tag{4.2}$$

$$\hat{G}_{27}^{(1)m,3P} = j_0(z) + \varepsilon j_1(z) + \mathscr{O}(\varepsilon^2), \tag{4.3}$$

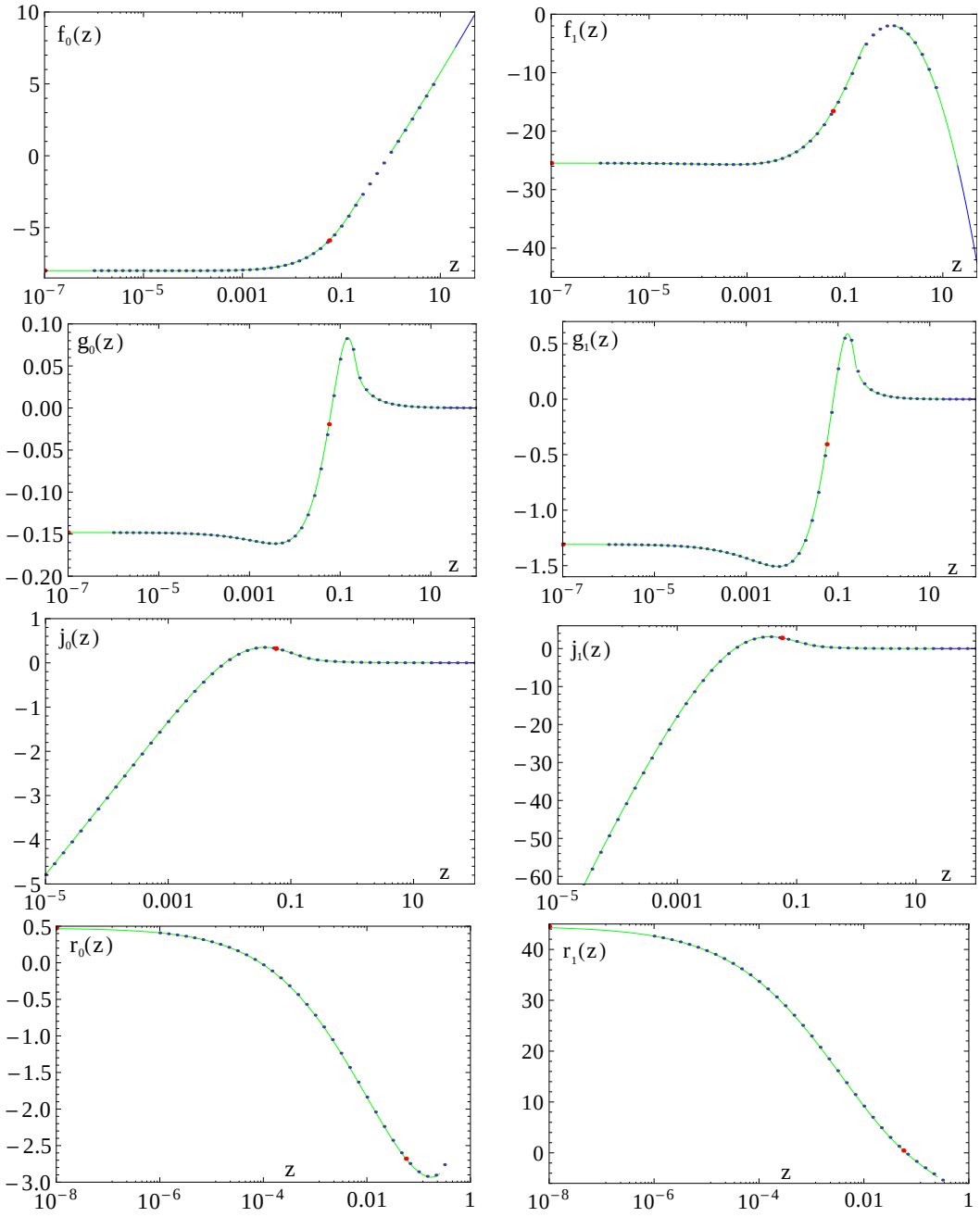

Figure 5: Plots of the functions defined in Eqs. (4.1)-(4.4). See the text.

$$\begin{aligned}\hat{G}_{27}^{(1)m,2P} &\equiv \hat{G}_{27}^{(1)m,2P(d)} + \hat{G}_{27}^{(1)m,2P(u)} \\ &= -\frac{1}{3\varepsilon^2} - \frac{1}{\varepsilon}\left(1 + \frac{4\pi^2}{81} + 2z\right) + r_0(z) + \varepsilon r_1(z) + \mathscr{O}(\varepsilon^2). \end{aligned} \tag{4.4}$$

Their dependence on z is displayed in Fig. 5. Each of the (blue) dots represents a particular final value of the numerical solution of the DEs. The physical point in the vicinity of $z = 0.06$ is marked by a bigger (red) dot. Similar (red) dots on the vertical axes show the limits at $z \to 0$ whenever

they are finite, i.e. for all the functions except $j_i(z)$. These limits are known from the $z=0$ calculation [2]:

$$\{f_0,f_1,g_0,g_1,r_0,r_1\} \xrightarrow{z\to 0} \Big\{-\tfrac{1942}{243},\ -\tfrac{26231}{729}+\tfrac{259}{243}\pi^2,\ -\tfrac{4}{27},\ -\tfrac{106}{81},\ \tfrac{35}{9}-\tfrac{161}{972}\pi^2-\tfrac{40}{27}\zeta(3),\quad \tfrac{2521}{54}+\tfrac{2135}{2916}\pi^2-\tfrac{65}{81}\zeta(3)-\tfrac{7}{81}\pi^4\Big\}. \quad (4.5)$$

A nice convergence to these limits is visible in our logarithmic-scale plots. In the case of $\hat{G}_{27}^{(1)m,3P}$, one finds [2, 22]

$$\hat{G}_{27}^{(1)m,3P}(z=0)=\tfrac{20}{27\varepsilon}+\tfrac{770}{81}+\left(\tfrac{18191}{243}-\tfrac{35}{27}\pi^2\right)\varepsilon+\mathscr{O}(\varepsilon^2), \quad (4.6)$$

which contains an $1/\varepsilon$ divergence, contrary to Eq. (4.3). It arises due to the logarithmic divergences of the functions $j_i(z)$ at $z\to 0$ [28]. Such non-commuting limits are often encountered in the framework of dimensional regularization.

The solid (blue) lines in the first six plots of Fig. 5 show the expansions in $1/z$ for $z>20$. They have served as the boundary conditions for the DEs at $z=20$. The remaining (green) solid lines describe expansions either in z (for $z<\frac{1}{4}$) or in $\frac{1}{z}$ (for $z>\frac{1}{4}$) that have been obtained in our analytical approach. For $f_i(z)$, the expansion plots are terminated away from the threshold at $z=\frac{1}{4}$ because they become inaccurate in its vicinity. In the three-body cases ($g_i(z)$, $j_i(z)$) the expansions are so accurate that their mismatch at $z=\frac{1}{4}$ is invisible within the plot resolution. The expansion depth in the small-z case was up to $\mathscr{O}(z^{30})$ and $\mathscr{O}(z^{15})$ for the three- and two-body contributions, respectively. Similarly, the large-z expansions were calculated up to $\mathscr{O}(1/z^{30})$ and $\mathscr{O}(1/z^{15})$ in the three- and two-body cases, respectively. All these terms are included in the plots. An exception is $g_0(z)$ for which we know (and plot) the fully analytical result:

$$g_0(z)=\begin{cases}-\frac{4}{27}-\frac{14}{9}z+\frac{8}{3}z^2+\frac{8}{3}z(1-2z)\,sL+\frac{16}{9}z(6z^2-4z+1)\left(\frac{\pi^2}{4}-L^2\right), & \text{for } z\le\frac{1}{4},\\ -\frac{4}{27}-\frac{14}{9}z+\frac{8}{3}z^2+\frac{8}{3}z(1-2z)\,tA+\frac{16}{9}z(6z^2-4z+1)A^2, & \text{for } z>\frac{1}{4},\end{cases} \quad (4.7)$$

with $s=\sqrt{1-4z}$, $L=\ln(1+s)-\frac{1}{2}\ln 4z$, $t=\sqrt{4z-1}$, and $A=\arctan(1/t)$. Our expansions in z and/or $1/z$ for all the other functions can be found in Refs. [21, 22].

In the cases of f_0, f_1 and g_0, our results are in agreement with Ref. [10]. As far as g_1 is concerned, no comparison is possible because our phase-space integrals have been evaluated in D dimensions, contrary to the four-dimensional approach of Ref. [10]. The method of reverse unitarity [29] that we apply in the IBP reduction makes the D-dimensional phase-space integration unavoidable.

5. Summary

We have determined the charm-quark mass dependence of all the necessary ultraviolet counterterm diagrams that contribute to the yet-unknown parts of the NNLO QCD corrections $\hat{G}_{17}^{(2)}$ and $\hat{G}_{27}^{(2)}$ to the weak radiative B-meson decay branching ratio. These corrections originate from interferences of the current-current ($Q_{1,2}$) and photonic dipole (Q_7) operators. At present, they are estimated using an interpolation in m_c, which generates one of the the main uncertainties in the perturbative contribution to $\mathscr{B}_{s\gamma}^{\rm SM}$.

The current experimental determination of $\mathscr{B}_{s\gamma}$ agrees with the SM prediction within uncertainties that are similar on the experimental and theoretical sides, and amount to around 7% each. A factor-of-two reduction on each side is feasible in the near future. In the experimental case, it is likely to come from high-statistics measurement using the hadronic tag for the recoiling B-meson, which essentially eliminates the so-called continuum background. Such measurements have been statistics-limited so far. On the theory side, the two main issues are re-considering the estimates of nonperturbative effects, and eliminating the m_c-interpolation in the perturbative NNLO contributions. Our calculation has contributed to a future resolution of the latter issue. However, a phenomenological use of our results will be possible only after determination of the bare NNLO contributions to the considered interference terms, namely $\hat{G}_{17}^{(2)\text{bare}}$ and $\hat{G}_{27}^{(2)\text{bare}}$.

A numerical calculation of the bare NNLO contributions is potentially achievable using the same techniques as described in the present work. However, it is considered a demanding task. In the two-particle-cut case alone, one encounters around 20000 scalar integrals, and around 500 MIs. Many yet-unknown single-scale MIs are expected to show up in the boundary conditions for the DEs in these calculations.

Acknowledgments

M.M. and A.R. acknowledge support from the National Science Centre (Poland) research project, decision no DEC-2014/13/B/ST2/03969.

References

[1] M. Misiak, H. Asatrian, R. Boughezal, M. Czakon, T. Ewerth, A. Ferroglia, P. Fiedler, P. Gambino, C. Greub, U. Haisch, T. Huber, M. Kamiński, G. Ossola, M. Poradziński, A. Rehman, T. Schutzmeier, M. Steinhauser and J. Virto, Phys. Rev. Lett. **114**, 221801 (2015) [arXiv:1503.01789].

[2] M. Czakon, P. Fiedler, T. Huber, M. Misiak, T. Schutzmeier and M. Steinhauser, JHEP **1504**, 168 (2015) [arXiv:1503.01791].

[3] Y. Amhis *et al.* (Heavy Flavor Averaging Group), arXiv:1412.7515; Additional information and updates: `http://www.slac.stanford.edu/xorg/hfag/` .

[4] K. Trabelsi, "Rare decays and exotic states in quark flavour physics," plenary talk at the EPS 2015 Conference, Vienna, Austria, July 22-29, 2015.

[5] M. Benzke, S. J. Lee, M. Neubert and G. Paz, JHEP **1008**, 099 (2010) [arXiv:1003.5012].

[6] T. Aushev *et al.*, arXiv:1002.5012.

[7] M. Misiak and M. Steinhauser, Nucl. Phys. B **764**, 62 (2007) [hep-ph/0609241].

[8] M. Misiak and M. Steinhauser, Nucl. Phys. B **840**, 271 (2010) [arXiv:1005.1173].

[9] R. Boughezal, M. Czakon and T. Schutzmeier, JHEP **0709**, 072 (2007) [arXiv:0707.3090].

[10] H. M. Asatrian, C. Greub, A. Hovhannisyan, T. Hurth and V. Poghosyan, Phys. Lett. B **619**, 322 (2005) [hep-ph/0505068].

[11] A. Ali and C. Greub, Z. Phys. C **49**, 431 (1991).

[12] C. Greub, T. Hurth and D. Wyler, Phys. Lett. B **380**, 385 (1996) [hep-ph/9602281].

[13] C. Greub, T. Hurth and D. Wyler, Phys. Rev. D **54**, 3350 (1996) [hep-ph/9603404];

[14] A. J. Buras, A. Czarnecki, M. Misiak and J. Urban, Nucl. Phys. B **611**, 488 (2001) [hep-ph/0105160].

[15] A.J. Buras, A. Czarnecki, M. Misiak and J. Urban, Nucl. Phys. B **631**, 219 (2002) [hep-ph/0203135].

[16] F. V. Tkachov, Phys. Lett. B **100**, 65 (1981).

[17] K. G. Chetyrkin and F. V. Tkachov, Nucl. Phys. B **192**, 159 (1981).

[18] S. Laporta, Int. J. Mod. Phys. A **15**, 5087 (2000) [hep-ph/0102033].

[19] A. V. Smirnov, JHEP **0810**, 107 (2008) [arXiv:0807.3243].

[20] A. V. Smirnov, Comput. Phys. Commun. **189**, 182 (2014) [arXiv:1408.2372].

[21] M. Misiak, A. Rehman and M. Steinhauser, in preparation.

[22] A. Rehman, Ph.D. thesis, University of Warsaw, 2015,
http://depotuw.ceon.pl/handle/item/1197 .

[23] A. V. Kotikov, Phys. Lett. B **254**, 158 (1991).

[24] E. Remiddi, Nuovo Cim. A **110**, 1435 (1997) [hep-th/9711188].

[25] T. Gehrmann and E. Remiddi, Nucl. Phys. B **580**, 485 (2000) [hep-ph/9912329].

[26] R. Harlander, T. Seidensticker and M. Steinhauser, Phys. Lett. B **426**, 125 (1998) hep-ph/9712228.

[27] T. Seidensticker, hep-ph/9905298.

[28] A. Rehman, Acta Phys. Polon. B **46**, 2111 (2015).

[29] C. Anastasiou and K. Melnikov, Nucl. Phys. B **646**, 220 (2002) [hep-ph/0207004].